Manuscript File

Click here to view linked References

Uncertainty in projected changes of Indian Summer Monsoon Rainfall by CMIP6 models

Sooraj K P[1], Pascal Terray[2] and Ajinkya M Aswale[1]

[1] Centre for Climate Change Research, Indian Institute of Tropical Meteorology, Ministry of Earth Sciences, Pune 411008, India

[2] Sorbonne Universites (UPMC, Univ Paris 06)-CNRS-IRD-MNHN, LOCEAN Laboratory, 4 place Jussieu, Paris, France

Submitted to Atmospheric Research

April 2025

Corresponding authors address:

Sooraj K. P.

Centre for Climate Change Research, Indian Institute of Tropical Meteorology

Pune 411008, India, https://orcid.org/0000-0003-1246-8922

e-mail: sooraj@tropmet.res.in

Abstract

A robust and trustworthy rainfall projection over the Indian landmass is vital for devising climate adaptation strategies. However, past studies show large inter-model spread in Indian Summer monsoon (ISM) rainfall projections thus calling for more detailed investigations on the underlying process. In the present study, we investigate this aspect using Coupled Model Intercomparison Project Phase 6 (CMIP6) model projections (Shared Socioeconomic Pathways, SSP5-8.5) and historical simulations. The Multi-Model Ensemble mean (MME) results show intensification of ISM rainfall at the end of the 21st century with ISM rainfall increasing by 1.6 ± 0.8 mm/day under SSP5-8.5 scenario. A moisture budget analysis for the MME further infers that the thermodynamic effect (TH) due to global warming plays a dominant role in enhancing ISM rainfall in the projections, with its dynamic counterpart (DY) assuming an additional contribution. It is also revealed that both DY and TH terms contribute to the model's uncertainty in ISM rainfall, but with DY dominating over the other this time. The model's uncertainty in DY and ISM rainfall changes is linked to inter-model spread in interhemispheric thermal contrast which in-turn depends on the diversity in Equilibrium Climate Sensitivity (ECS) and Global Mean Temperature (GMT) among the models. Intriguingly, when we remove the inter-model diversity in ECS through a GMT scaling, an Atlantic meridional surface temperature gradient, involving both land and ocean, emerges as a crucial driver in controlling the uncertainty in both DY and ISM rainfall changes, and drives large-scale monsoon circulation changes over African and the Indian subcontinents.

Keywords: ISM future projection uncertainty; GMT; ECS; DY; TH; moisture budget; interhemispheric thermal contrast; Atlantic meridional surface temperature gradient

1. Introduction

South Asian Summer Monsoon system provides freshwater resources for the most densely populated regions of South Asia and hence considered to be a crucial component of the Global Monsoon system (e.g., Webster et al 1998; Wang and Ding 2006). In particular, the vagaries of Indian Summer Monsoon (ISM) rainfall at different time scales have a significant influence on the well-being of the Indian people by dominantly contributing to the mean annual precipitation over the Indian land mass. In this context, the aberrations in ISM rainfall behaviour with frequently occurring rainfall extremes make the Indian subcontinent highly vulnerable to the ongoing climate change (IPCC 2021). Thus, assessing the response of ISM rainfall and narrowing its uncertainties in global warming projections is crucial for devising future strategies, planning and adaptation measures, but remains a challenging scientific task (Douville et al 2021; Jin et al 2020; Rajesh and Goswami 2022).

Climate change future projections are subject to large uncertainty (e.g., Hawkins and Sutton 2009; Lehner et al 2020). There are three sources of uncertainties. First one is related to the uncertainty from internal variability arising due to the chaotic nature of the climate system. Second one is model uncertainty based on the premise that the climate response changes from model to model due to differences in spatial resolution, parameterized/missing processes among the models. Third one is scenario uncertainty due to the unknown future greenhouse gas emissions and the associated uncertainty in radiative forcing. The focus here is on the model uncertainty as it is the dominant factor in the highest scenario and in all the long-term future projections (Zhou et al 2020; Lehner et al 2020).

The recent Intergovernmental Panel on Climate Change Assessment Report (IPCC 2021; Douville et al 2021) inferred that the ISM rainfall is projected to intensify at the end of the 21st century. However, there exist large model-dependent uncertainties in the ISM rainfall projections as manifested by substantial inter-model spread among the state-of-the-art climate

model projections (e.g., Douville et al 2021; Jin et al 2020; Rajesh and Goswami 2022). In other words, the climate models show notable disagreements in rainfall projections (for magnitude of rainfall changes), which persist from Coupled Model Intercomparison Project phase 3 (CMIP3) to CMIP6 (e.g., IPCC 2001, 2007, 2013, 2021; Li et al 2017; Chen et al 2020; Rajesh and Goswami 2022). Furthermore, this model uncertainty is not decreasing from one CMIP exercise to the next, despite some model improvements.

As expected from the Clausius-Clapeyron relationship, the global warming leads to enhanced evaporation due to increased water vapor and moisture content in the atmosphere, thus increasing ISM rainfall (e.g., May 2002; 2011; Ueda et al 2006; Cherchi et al 2011; Endo and Kitoh 2014; Kitoh et al 2013; Menon et al 2013; Ma and Yu 2014; Sharmila et al 2015; Sooraj et al 2015; Kulkarni et al 2020; Douville et al 2021). But some of these studies also reported a weakening of the monsoon circulation, thus complicating the rainfall responses and leading to the well-known "monsoon paradox" (e.g., Ma and Yu 2014).

Some studies have examined the processes contributing to this model's uncertainty in rainfall projections by splitting the rainfall change into two components: thermodynamic response associated with moisture change and dynamic response associated with monsoon circulation change (e.g., Seager et al 2010; Huang et a 2013; Endo and Kitoh 2014; Sooraj et al 2015; Li et al 2017; Chen et al 2020; Long and Li 2021). It is subsequently inferred from these previous studies that while the thermodynamic processes are responsible for the future rainfall intensification, the dynamic component tends to offset this rainfall increase owing to a slowdown of the monsoon circulation (Chen and Zhou 2015), at least at mid-tropospheric levels (Ma and Yu 2014). Moreover, the dynamic component exhibits a huge inter-model spread in contrast with its thermodynamic counterpart and, accordingly, it is suggested that the uncertainty in rainfall projections arise due to the dynamic component (e.g., Ma and Yu 2014; Sooraj et al 2015; Chen and Zhou 2015; Li et al 2017; Chen et al 2020).

The peculiar Sea Surface Temperature (SST) Indo-Pacific warming patterns are also proposed as another key factor that contributes to the uncertainty in ISM rainfall projections (Chen and Zhou 2015; Xie et al 2015; Long et al 2016). According to Chen and Zhou (2015), these Indo-Pacific warming patterns modulate both the zonal tropospheric temperature gradient over the ISM region and the interhemispheric moisture transport, thus explaining the inter-model spread of projected ISM rainfall. Other studies have attributed the ISM rainfall projection uncertainty to the inter-model difference in land-sea thermal contrast and associated low-level monsoon circulation (Ma and Yu 2014; Endo et al 2018; Wang et al 2020; Jin et al 2020).

In particular, the aforementioned weakening of the monsoon circulation is found to be associated with various factors. Firstly, the reduction in meridional land–sea thermal contrast in the upper troposphere is shown to be slowing down the mean monsoon circulation (Ueda et al 2006; Sun et al 2010; Dai et al 2013; Wu et al 2023; Luo et al 2024). Second, another proposed mechanism, the warm-get-wetter effect (Huang 2014), links central to eastern Pacific SST warming and associated local rainfall changes with a modulation of the Indo-Pacific Walker circulation causing the weakened monsoon circulation (May, 2004, 2011; Li et al 2022); in other words, the projections that produce an El-Nino like warming pattern in the Pacific mean-state promote reduced ISM rainfall by teleconnections similar to the ENSO-ISM rainfall relationships at the interannual time scale (Guilbert et al 2023). Third, Ma et al (2012), Ma and Yu (2014) and Ma et al. (2018) have later suggested a Mean Advection of Stratification Change (MASC) mechanism through which the enhanced atmospheric static stability under anthropogenic forcing promotes cooling/heating in the convective ascending/subsidence regions, thus weakening the mean atmospheric circulation. According to them, the MASC weakens the upper tropospheric circulation while the enhanced surface land-sea contrast

strengthens the lower-level winds thus leading to another "monsoon paradox" and large compensating effects occur between these two features.

In summary, the sum of several important opposing effects, both dynamic and thermodynamic eventually dictates the future rainfall response, thus adding large complexity to estimate the future ISM characteristics with fidelity, which gets further translated into large inter-model diversity in future ISM projections.

In this study, we incorporated multiple diagnostics to analyse the projected changes in ISM rainfall and the associated uncertainties using CMIP6 models. The following points underpins our study: (1) To disentangle the main physical processes associated with the ÍSM rainfall changes in future projections, (2) To unravel the sources of uncertainty in the projected ISM rainfall, (3) To bring out the main physical factors contributing to the uncertainty in projected ISM rainfall in CMIP6 models.

Section 2 provides the data and methodology as used in the study. Section 3 describes the future changes in ISM characteristics. Section 4 examines the origin of uncertainty in future ISM rainfall projections. Finally, it ends with a comprehensive summary in Section 5.

2. Data and Methods

2.1 CMIP6 simulations

This study is based on historical and highest emission Shared Socioeconomic Pathways (SSP5-8.5, simply SSP585) scenario experiments from 30 coupled models contributing to CMIP6 (Eyring et al. 2016; O'Neill et al. 2016). See Table 1 for a general overview of the model datasets. The historical runs of CMIP6 models are forced with the natural and anthropogenic forcings (Eyring et al. 2016), while the SSP585 scenario depicts the highest emission scenario where the radiative forcing reaches 8.5 W/m^2 by 2100 (O'Neill et al. 2016). Here we have used the first available ensemble member (i.e., either r1i1p1f1 or r1i1p1f2) from

each model. In other words, we used one member simulation for each model in contrast to multi-member averaging under the assumption that the inter-model spread is largely driven by changes in the forced response of the models rather than internal variability when the focus is on the mean-state and long-term changes of the monsoons (Guilbert et al 2023, 2024).

We used the monthly mean outputs from CMIP6 archives as obtained for various atmospheric variables: rainfall (P), surface temperature (TS), mean sea-level pressure (MSLP), specific humidity and horizontal winds (U and V). The monthly mean datasets from all CMIP6 models are bilinearly interpolated into a 1° × 1° grid for ease of comparison. Our analysis focuses on the period 1979–2013 for the historical simulations and the period 2065-2099 for the SSP scenario, and the diagnostics are performed mainly for the boreal summer season (June to September, JJAS) period, using both the historical and SSP simulations. The 1979–2013 mean in historical simulations defines the present-day reference climatology, while the 2065–2099 mean in SSP585 defines the climatology at the end of 21st century and their difference represents the future change. Note that the datasets (i.e., data from historical and SSP separately) are not linearly detrended before estimating the future change. Also, note that the aforementioned choices of SSP585 and the long-term future changes (i.e., end of 21st century changes), are made as it may reveal more clearly the model uncertainty as already stated in the Introduction (Lehner et al 2020). Finally, in order to point out the systematic errors in CMIP6 simulations as relevant to the rainfall in and around ISM region, we have also used a global monthly mean precipitation dataset with a horizontal resolution of 2.5°×2.5° (here interpolated to 1° × 1° grid), as obtained from the Global Precipitation Climatology Project (GPCP) monthly precipitation analysis for the period from 1979 to 2013 (Adler et al. 2018).

2.2 Definition of key climate and ISM indices

The study also used various climate indices as defined over specific regions for illustrating and interpreting the results. Firstly, it used the ISM rainfall index as rainfall averaged over the region between 8°N to 22°N and 70°E to 85°E (i.e., containing both land and ocean grid points). Secondly, it used a global interhemispheric surface skin temperature (TS) gradient with respect to the latitude 25°N (here after referred as IHTG) as our main focus is on the boreal summer season. To be precise, it is defined as the difference between TS averaged over the region to the north (i.e., over 25°N to 90°N and 0° to 360°E) and south (i.e., over 60°S to 25°N and 0° to 360°E) of 25°N. Besides these, the study has also used other temperature and monsoon dynamic based indices. First one is the meridional TS gradient signature over the Atlantic sector (AMTG), defined as North Atlantic TS over 40°W-10°W, 25°N-65°N minus South Atlantic TS over 40°W-10°W, 25°S-5°N. The justification for using these global and regional temperature indices will become clear as we proceed further (see Section 4). Note also that slight changes in the definition of these indices do not change the main results and inferences.

Secondly, to assess the dynamical characteristics of ISM, we used three indices. First one is the low-level zonal wind (at 850-hPa) averaged over the Arabian Sea domain (10°N–20°N, 55°E–65°E) reflecting the intensity and core of low-level westerlies (i.e., low-level jet, LLJ core or simply NLLJ, Wilson et al 2018). For a better illustration of the response of the ISM low-level circulation under the climate change forcing, we also used another zonal wind (at 850-hPa) index as averaged over a domain south of the LLJ position (i.e., SLLJ over Eq–10°N, 55°E–65°E). Next, for monitoring the changes in the strength of the upper tropospheric circulation, i.e., Tropical Easterly Jet (TEJ), we used a zonal wind index at 200hPa averaged over its core intensity region (40°E-100°E, 10°S-20°N, Abish et al 2013). These indices are further tabulated in Table 2 for easy reference.

2.3 Equilibrium Climate Sensitivity (ECS)

The ECS measures the eventual long-term global mean temperature or global mean warming rate in response to doubled CO_2 concentration relative to the pre-industrial period (Meehl et al 2020). The ECS values for all models (except for 4 models: FIO-ESM2, IITM-ESM, NorESM2- MM and EC-Earth3-CC) are derived from the Table 2 in Meehl et al (2020), as calculated by them using CMIP6 models based on its availability until march 2020. While the ECS for FIO-ESM2-0 is derived from Table B2 of Williamson et al (2024), the values for other three models are taken from the Supplementary excel data of Hausfather et al (2022). As per the studies, the ECS is computed by regressing the net top-of-atmosphere radiance against the global mean surface air temperature changes in the first 150 years of the CO_2 quadruples experiment (Gregory et al 2004; Forster et al 2013; Meehl et al 2020; Chen et al 2022).

2.4 Moisture budget analysis

To further understand the changes and uncertainty in the ISM rainfall projections, the moisture budget analysis and its decomposition is incorporated, following formulations from earlier studies (Chou et al 2009; Endo and Kitoh 2014; Sooraj et al 2015; 2016; Chen et al 2020).

The vertically integrated anomalous moisture equation is written as

$$P' = E' - \partial_t\langle q\rangle' - \langle\overrightarrow{u_h}\cdot\nabla q\rangle' - \langle q\nabla\cdot\overrightarrow{u_h}\rangle' + RES \qquad (1)$$

where the angle brackets indicate vertical integration through the entire troposphere, the primes denote the anomalous future changes relative to the reference climatology from historical simulation (i.e., histclim) and ∇ is the horizontal gradient operator. The variable q denotes specific humidity, while $\overrightarrow{u_h}$ denote horizontal wind. The terms E and P are evaporation and rainfall, respectively. While the term $-\langle\overrightarrow{u_h}\cdot\nabla q\rangle'$ represents horizontal moisture advection, $\langle q\nabla\cdot\overrightarrow{u_h}\rangle'$ stands for moisture convergence. Final term on the right-hand side is residual (RES).

The RES term accounts for contributions from non-linear interaction between anomalous circulation and moisture, and is assumed to be small (Zhang and Li 2022; Chen et al 2024a). Note also that the daily transient eddies terms and their contributions are not investigated in this study considering their negligible contributions to the long-term budget changes (Zhang and Li 2022 and the references therein). The time derivative of specific humidity, $\partial_t\langle q\rangle'$, is also ignored here considering the longer seasonal mean time scale. Earlier studies noted that the regional mean horizontal moisture advection is often negligibly small compared to other moisture budget terms, at least for ISM (e.g., Jin et al 2020). With all these assumptions, the Eq. (1) can be further approximated as following:

$$P' = E' - \langle q\nabla\cdot\overrightarrow{u_h}\rangle' + RES \qquad (2)$$

The moisture convergence can be further decomposed as follows:

$$-\langle q\cdot D\rangle' = -\langle q_{histclim}\cdot D'\rangle - \langle q'\cdot D_{histclim}\rangle \qquad (3)$$

In Eq. (3), D' represents future change in divergence ($\nabla\cdot\overrightarrow{u_h}$), and, accordingly, the two terms on the right-hand side represent the dynamic and thermodynamic components, respectively. While the dynamic contributions (DY) are related to the future changes in atmospheric circulation, the thermodynamic contributions (TH) are related to the changes in moisture content.

Finally, the results are mostly presented using Multi-Model-Ensemble (MME) mean of 30 models and illustrated using several ways. The usually well-known statistics such as inter-model Standard Deviation (SD) and Signal to Noise Ratio (SNR) are used to measure the source of model uncertainty in future projections. SNR is the normalised future change signal with inter-model SD. Then, standard scatter plots and correlation/regression analysis are also conducted to detect the relationships between the aforementioned climate indices and to decipher the dominant spatial pattern of model's uncertainty in future rainfall projections across the various models, respectively. Finally, the statistical significance of the correlation

coefficients was determined based on a two tailed Student's t-test (Storch and Zwiers, 2002), assuming that the model realisations are independent.

3. Future changes in ISM rainfall during the twenty-first century

Figures 1a, c show future changes of boreal summer rainfall and low-level circulation over the Indian sector based on the MME of 30 CMIP6 models (see Section 2). The rainfall pattern across the Indian domain shows a tilted dipole structure with significant rainfall enhancement (suppression) over the ISM (southeastern Indian Ocean) region. Similar asymmetric rainfall structure is noted in earlier CMIP based studies as well (e.g., Srivastava and DelSole 2014; Sooraj et al 2015; Sharmila et al 2015). In particular, according to Srivastava and DelSole (2014), the dominant mode associated with future ISM change reveals a dipole pattern as demonstrated by applying discriminant analysis to future rainfall changes over South Asian Summer monsoon region. While the enhanced rainfall signature extends over a big region covering the Indian Ocean North of the Equator, the rainfall decrease is mainly confined to the Inter-Tropical Convergence Zone (ITCZ) over Indian Ocean (i.e., over southeastern equatorial region). The noted rainfall intensification over the southwest Arabian Sea suggests anomalous westward extension of rainfall in the future projections. These signatures imply non-uniform future response in the multiple regional heat sources or local rainfall maxima, centred over the Indo-Bay of Bengal, the tropical western Pacific and the eastern equatorial Indian Ocean.

However, there is uncertainty for the rainfall projections across the Indian monsoon domain. In particular, it shows large inter-model SD over many regions across India even exceeding the rainfall changes, thus leaving low SNR values (≤ 1) (see Fig 1a-b). Figure 1d further exemplifies the large inter-model spread over ISM region with a wide range of future rainfall responses (ranging from 0.2 mm/day to 4 mm/day). Recently, Guilbert et al (2024)

inferred that the magnitude of model uncertainty (e.g., inter-model SD) is larger than the future rainfall changes in most of the tropical regions. According to them, in particular, there is large uncertainty in future rainfall projections over Sahelian and Indian monsoon regions consistent with previous studies as well (Monerie et al 2017; Zhang and Li 2022).

Figure 1a further shows anomalously strong low-level westerlies to the north of 10°N while there are pronounced easterly anomalies along the equator. The strong westerlies imply the future intensification in LLJ core (as defined over the Arabian Sea, 10°N–20°N and 55°E–65°E following Wilson et al. 2017, see Section 2 for more details), as demonstrated in Figure 2a across all the models. On the other hand, prominent anomalous easterlies along the equator suggests the weakening of climatological westerly flow between equator to 10°N (Kitoh et al. 1997; Ashrit et al. 2005; Sooraj et al 2015; Chen et al 2024a): i.e., weakening of low-level westerly component over the Arabian Sea region to south of the LLJ core (Eq–10°N, 55°E–65°E, see Section 2 for more details), as further exemplified in Figure 2b across the models. This north-south dipole low-level wind signature further point toward the poleward shift in LLJ in future projections (e.g., Sandeep and AjayaMohan 2015, Chen et al 2024a). Figure 2a furthermore illustrate that this poleward shift is consistent across all the models, on similar lines with the aforementioned asymmetrical rainfall changes in Figure 1a, i.e., decrease (increase) of rainfall over south-east Indian Ocean (ISM) regions, thus inferring that the monsoon circulations are fundamentally coupled with the regional convection shifts (e.g., Back and Bretherton 2006; Ma et al 2018). A recent study using CMIP6 projections (Chen et al 2024a) also showed poleward shift in zonally averaged overturning Hadley circulation which they attributed to the future enhancements in ISM rainfall.

We next performed a moisture budget analysis to gain further understanding on projected ISM rainfall changes and to quantify the relative contributions of DY and TH terms to the projected ISM rainfall changes based on its decomposition in Equation 3. The DY and

TH components for the MME are displayed as a box-whisker in Figure 3a along with other terms (PR, E and residual), as averaged over ISM region. All the budget terms (except for residual) show positive contribution to the ISM rainfall change though the contribution from evaporation is relatively minor, while the impact due to residual term is negligible thus increasing confidence in the moisture budget estimates in Figure 3a.

It is well-known that the TH component robustly contributes to the ISM rainfall intensification following the Clausius-Clapeyron equation as the atmospheric moisture content increases under a warming climate (Held and Soden 2006; Cherchi et al 2011; Li and Ting 2017; Jiang et al 2023). Consistent with this, the results from MME show that the enhanced ISM rainfall is primarily contributed by the increase in TH term (Fig 3a). Recent CMIP based studies also found similar inferences on global and regional monsoon rainfall projections as dominated by the increase of moisture (TH, e.g., Endo and Kitoh 2014; Chen and Zhou 2015; Sooraj et al 2015; Chen et al 2020). Interestingly, our results show additional positive contribution from DY (albeit a secondary role) as well, thus implying that both the DY and TH components are contributing to the future ISM rainfall increase. This is further revealed if one sees the wetting and drying tendency at the individual model level. To be precise, while the TH component promotes ISM rainfall intensification in most models (with an exception in only one model), approximately, two thirds of model projections (22 out of 30) show wetting effect due to DY. The distinct wetting response by dynamical component can be further elucidated by the enhanced circulation response in the future as shown in Figure 2a for the NLLJ (i.e., low-level zonal wind averaged over Arabian Sea, 10°N–20°N, 55°E–65°E as defined in Section 2). As demonstrated in Figure 2a, most of the CMIP6 models show enhanced low-level westerlies over the Arabian Sea in future projections and hence accounting for enhanced low-level convergence as associated with the DY component. Ma and Yu (2014) also inferred that the strengthening of low-level circulation and increase in moisture have both contributed to the

intensification of ISM rainfall in previous CMIP's models. According to them, the upper-level circulation shows weakening in the future in contrast to the lower wind response, thus illustrating the paradoxical behaviour between upper and lower-level monsoon circulations, as further shown in Figure 2a. However, there is large inter-model spread both in lower and upper tropospheric circulations coinciding with the larger uncertainty in DY component. Interestingly, these two contrasted signatures at low- and upper-levels (e.g., strengthening and weakening) are further found to be significantly coupled across the models (showing a correlation of 0.33 significant at the 95% confidence level, see Fig. 2b).

Considering the poleward shift in LLJ as found to be intrinsically coupled to local convection patterns and as manifested in the dominant dipole rainfall mode over South Asian monsoon region, we did similar moisture budget (using Eq. 3, see Fig. 3b) over south-east Indian Ocean region (20°S-Equator, 70°E-100°E) to account for the suppression of rainfall over this region and a better understanding of the underlying ISM dynamics. The MME results show that similar to ISM domain, the contributions from evaporation and residual terms are relatively minor. The DY term predominantly contributes to cause the local dryness thus accounting for the future reduction in rainfall over south-east Indian Ocean region. There is contribution from TH as well though, but it is modest compared to DY. It is important to note that the south-east Indian Ocean being a regional primary convection centre (i.e., ITCZ associated) is climatologically an ascending region (Sooraj et al 2015) and hence the contributions of DY to total future rainfall changes must be strongly negative to produce rainfall suppression over there as conspicuously observed from Figure 3b as well. This explains the predominant role of DY term (relative to TH) in causing rainfall suppression over south-east Indian Ocean region which is further consistent with the aforementioned weakening of low-level westerlies over the Arabian Sea region (i.e., SLLJ, see Fig. 2a), thus partially explaining the dipole rainfall pattern over South Asian monsoon region by the northward shift of the LLJ. Interestingly, both

evaporation and residual terms show a wetting effect over south-east Indian Ocean region, thus modestly counteracting the combined drying effect due to DY and TH terms.

Earlier investigations on ISM rainfall using CMIP5 future projections inferred that the effect of DY is to completely offset the dominant wetting effect by its thermodynamic counterpart as manifested by all models consistently showing compensation between dynamic and thermodynamic effects (Endo and Kitoh 2014; Chen and Zhou 2015; Sooraj et al 2015). In contrast, as per our results, the DY component in most of the CMIP6 models shows enhancing effect thus promoting ISM rainfall. However, a point to be noted is that some of the CMIP6 models still exhibit counterbalancing behaviour in DY component (i.e., DY counteracting the dominant wetting) as obvious from Figure 2a and 3a. This implies that the effect of DY (i.e., drying and wetting changes) varies widely across the CMIP6 projections and hence the behaviour of DY has drastically changed from its predecessor generation of CMIP (i.e., CMIP5 models showing predominantly and uniformly drying DY effect; Chen and Zhou 2015; Sooraj et al 2015). This non-uniform behaviour in DY term (unlike TH) across the CMIP6 models is further translated into relatively larger inter-model spread which needs further exploration to decipher the underlying process as done in the following sections.

4. Driving factors of model's uncertainty in future ISM rainfall projections

4.1 Interpreting ISM rainfall uncertainty using dynamic (DY) and thermodynamic (TH) components

Here firstly, we assess in more details the inter-model spread in moisture budget terms to gain further insights on the projected uncertainty in ISM rainfall. Firstly, the DH component exhibits the highest inter-model spread among the moisture budget terms with evaporation showing relatively smaller inter-model SD (see Table 3). The residuals also show moderately high spread, but less to the spread of both DY and TH, suggesting that their contributions to the

ISM rainfall uncertainty are not the driving factors to first order. Furthermore, regarding the residuals in the atmospheric moisture budget, Paula and Kummerow (2014) noted that balancing moisture budgets is a challenging task, in particular, at regional scales.

Based on SNR, the TH component displays the largest ratio (1.9) comparable to the SNR estimates from the ISM rainfall projections (see Table 3). In contrast, the uncertainty in DY component is exemplified by the lowest SNR value (less than 1) compared to other dominant budget components. The contrasting SNR statistics between the DY and TH components in-turn imply relatively higher model consistency for the later one in causing the ISM rainfall intensification in the future.

Inter-model correlation is then performed to have further insights on the above diverse behaviour across the models and to account for the uncertainty in ISM rainfall. Figure 4a shows the inter-model relationship between ISM rainfall change and DY, whereas a similar plot is shown in Figure 4b by replacing the dynamic with its thermodynamic counterpart (TH). The DY component demonstrates a significantly high correlation coefficient (0.81, see Fig 4a) with the ISM rainfall change, inferring that the inter-model diversity in the DY component definitely dominates the inter-model spread in ISM rainfall change and hence drives its uncertainty. However, one cannot also rule out a secondary, but still significant, role from the thermodynamic component (with a significant correlation value of 0.50 at 95% level of significance, see Fig 4b) in contributing to uncertainty in ISM rainfall change. So, it is inferred that both the DY and TH components jointly account for the uncertainty in ISM rainfall projections, but this uncertainty is largely dominated by DY.

4.2 Underlying physical mechanisms

It is previously inferred that the inter-model spread in the global warming levels (i.e., global mean temperature, GMT) partially accounts for the above highlighted projected

uncertainties (Chen and Zhou 2015; Chen et al 2020). As an illustration, it is very common to express rainfall changes per °C of global warming in past monsoon or tropical studies (e.g., Held and Soden 2006; Chou et al 2009; Chou et al 2012; Cherchi et al 2011; Huang 2014; Chen and Zhou 2015; Zhang and Li 2022; Jiang et al 2023; Guilbert et al 2024) based on a hypothetical Clausius-Clapeyron scaling (i.e., scaling by GMT) and the increase of precipitable water associated with a warmer tropical atmosphere. Is this scaling framework valid for the ISM rainfall changes?

So, as a next step, we explore the association of DY and TH components over ISM region (along with ISM rainfall) to the future change in GMT, thus demonstrating their eventual partial sensitivity to global warming levels (Fig 5a-c). A significant linear relationship is manifested between GMT and DY (r=0.3, significant at 95% confidence level) thus dominantly explaining the relationship of GMT with ISM rainfall (r=0.4, Fig 5a-b). In contrast and contrary to the expected Clausius-Clapeyron scaling, TH shows only a weak and insignificant sensitivity to GMT (Fig 5c) challenging the validity of the Clausius-Clapeyron scaling for the ISM region. Additional analysis reveals that the inter-model diversity in GMT is further strongly and significantly linked to the global mean warming rate under a long-term equilibrium climate response (figure not shown, with a highly significant correlation coefficient of 0.88), as usually called in the literature as ECS (equilibrium climate sensitivity, see Section 2 for more details). Stated differently, and as expected, the models with a higher ECS tend to show a greater GMT in the SSP585 projections.

Considering the close association between GMT and ECS, it makes sense to further analyse the association between ECS and the dominant moisture budget terms (Fig 6). Interestingly, both DY and ISM rainfall components are more strongly and significantly associated with ECS (r=0.47 for ISM rainfall and r=0.37 for DY, both significant at 95% confidence level, see Fig 6a-b), while the TH term is now nearly insensitive to ECS with a

weaker association (r=0.07) than the one found with GMT. The implication is that the GMT through inter-model spread in ECS partially contributes to the projected uncertainty in DY term which in turn partially accounts for the model's uncertainty in ISM rainfall. These results assume significance as CMIP6 models are known to differ more in their ECS than their CMIP5 counterparts (Forster et al 2021; Hausfather et al 2022).

Now a question arises: through what physical process the ECS (or GMT) is linked to uncertainty in ISM rainfall across the models since Clausius-Clapeyron scaling is no longer the dominant factor? To explore this aspect, we carried out the inter-model correlation analysis between TS changes and the ISM averaged rainfall changes (see Fig 7a). Note that for ease in interpretation, assuming that ISM rainfall and dynamic changes may be more influenced by temperature gradients and/or local convective instability, the GMT change is subtracted from the TS change at every grid point for each model before doing the inter-model correlation analysis displayed in Figure 7a. Note also that we did similar correlation analysis using DY and TH components averaged over ISM region and the results for DY term are similar to those with ISM rainfall changes, consistent with previous results (figures for both are not shown here for brevity).

Figure 7a shows a well-defined global interhemispheric contrast in TS with anomalous future warming (cooling) north (south) of 25°N. There are prominent "regional" meridional TS gradient signatures across the Atlantic region as well and we will revisit this regional aspect later. The interhemispheric TS gradient (IHTG, defined in Section 2 as the difference between TS zonally averaged between 25°N to 90°N and 60°S to 25°N) is subsequently found to be strongly sensitive to ECS (r=0.63, see Fig 6d) and hence to GMT (r=0.5, significant at 95% level of significance, figure not shown) as well. Moreover, the IHTG is found to be significantly correlated with ISM rainfall changes (r=0.51, significant at 95% level of significance, Fig. S1) as well as with DY (r=0.4, significant at 95% level of significance) and TH (r=0.33, significant

at 95% level of significance) components. This in conjunction with the aforementioned significant association of DY and ISM rainfall with both ECS and GMT (see Fig 6a-b), gives an interpretation that the sensitivity of ISM rainfall to the inter-model spread in ECS (or GMT) can be mainly explained through the contributions from the DY. Furthermore, the contribution from the DY component is possibly linked to the IHTG, which increases with GMT and ECS across the models. This IHTG is usually interpreted as a proxy for inter-hemispheric energy transports in the atmosphere and a large-scale factor controlling the ITCZ migration towards the warmer hemisphere as achieved through the interhemispheric energy transport (e.g., Schneider et al 2014; Byrne et al 2018; Biasutti et al 2018). In other words, the monsoon rainfall and its associated circulation changes under anthropogenic CO_2 forcing is basically driven by interhemispheric thermal contrast (IHTG) due to the interhemispheric radiative imbalance between the two hemispheres, thus causing a migration of ITCZ toward the hemisphere with the greater heating. Recently, Guilbert et al (2024) invoked a similar mechanism to account for the inter-model spread in Sahel rainfall projections. According to them, the modulation of IHTG across the models leads to changing latitudinal positions of ITCZ and, consequently, varying Sahel rainfall intensity. The importance of IHTG onto Global Monsoon model's uncertainty is further demonstrated in a recent study focusing on atmospheric energy transport (Chen et al 2024b). These results connecting the in-phase association between interhemispheric transport and the ISM rainfall are also in line with the driving role of the "direct radiative forcing" through enhanced low-level monsoon circulation (Li and Tung 2017; Endo et al 2018).

However, the GMT and ECS through the global IHTG is not expected to fully account for the larger inter-model spread in rainfall projections, as Fig S1a implies that only ~30% (r=0.5) of the inter-model spread in ISM rainfall projection is explained by the global IHTG. This suggests that other factors are also at play to determine the ISM rainfall uncertainty as investigated next.

To completely ascertain this aspect, we further carried out an inter-model correlation analysis, similar to Figure 7a, but after applying the scaling method using GMT (i.e., both the ISM rainfall and TS changes are divided by GMT for each model before performing the correlation analysis). Incorporating GMT scaling to account for the large variation of (global) GMT across the models (see Fig 7b), revealed an interestingly different regional picture. The correlations across the globe have now completely disappeared, with no clear interhemispheric TS signatures unlike in Figure 7a. Additionally, there is almost no significant TS signatures over the tropics, in particular over subtropical Arid (i.e. to the west of ISM region), west Pacific, and equatorial Pacific domains. Interestingly, Figure 7b shows a prominent exception over north and south Atlantic regions, which further exhibits a well-defined meridional TS gradient signature across Atlantic, thus revealing a significant association with the inter-model spread in ISM rainfall change, even after scaling with GMT. Note that these signatures were robust in Figure 7a as well. Hence the meridional TS gradient signature over Atlantic (AMTG, as defined in Section 2 as North Atlantic TS over 40°W-10°W, 25°N-65°N minus South Atlantic TS over 40°W-10°W, 25°S-5°N) may be an emerging factor accounting for the uncertainty in ISM rainfall in addition to ECS (or GMT), which may be consistent with many past studies linking the interannual variability of ISM rainfall with SST variations in the Atlantic sectors, especially in the context of global warming (e.g., Liu et al 2014; Vital et al 2020; Yang and Huang 2021; Zhang and Li 2022; Sooraj et al 2023; Terray et al 2023).

In light of the above hypothesis, we further carried out new analyses based on Atlantic TS indices. The scaled Atlantic Meridional TS gradient (AMTG) changes show a prominent correlation with the inter-model spread of scaled ISM rainfall change as well as with the DY component (see Fig 8a-b, r=0.4, significant at 95% confidence level), with north Atlantic (r=0.4, not shown) region contributing more to the uncertainties in the ISM rainfall projections

than its southern counterpart (r=-0.26). In contrast, the TH term does not show any significant association with AMTG (see Fig 8c).

Figure 9a further shows that models with an enhanced AMTG in the future projection leads to strengthening of subtropical highs in southern Atlantic region with opposite signature in the north Atlantic as expected from an enhanced inter-hemispheric transport associated with a (regional) energy imbalance. At regional level, one can also see well defined MSLP gradients and associated low-level atmospheric flow in particular over the Afro-Asian sector (see Fig 9a). This is further manifested in the intensification of lows extending from the Sahara to the Arabian Peninsula, as consistent with a westward shift of the monsoon circulation (Terray et al 2018; Sooraj et al 2019, 2020). Associated with this strengthened large-scale subtropical low, there is a significant intensification of winds coming from the Gulf of Guinea in agreement with geostrophic balance. The winds, reinforced by the low, then interact with the ISM circulation through the Somali jet off the African coast (Fig 9a). The strong convergence of surface winds over the northeastern Arabian Sea also increases the moisture flux towards the western Indian Ocean and western India. In consonance with this, there is an intensification of the African (Sahelian) and Indian monsoons as demonstrated in Figure 9b with enhanced rainfall concentrated in between 10°N and 20°N. In particular for the ISM, there is increase in rainfall over the western Arabian Sea (i.e., on the windward side of the Ghats) and along the southern part of Indo-Gangetic plains. Hence, a larger projected increase of AMTG brings a stronger low-level cross equatorial moisture transport thus leading to increase in Sahelian-Indian monsoon rainfall in the future. More precisely, there is a southwest-northeast contrast in rainfall over ISM region and a northward shift of the ITCZ over Africa for Sahelian monsoon. Interestingly, a dipole signature in rainfall (as noted earlier) is manifested here as well, though less pronounced, implying that the AMTG is able to partially explain the future rainfall spread not only over ISM region but also over the neighbouring south-east Indian Ocean.

Importantly, the aforementioned atmospheric signatures (as seen in Fig 9a) are broadly similar to those associated with the ISM rainfall future changes itself as illustrated in Fig 9c. In particular, it shows the strengthening of southern hemispheric subtropical highs across the Atlantic region and a gigantic low extending from Sahara to the Arabian Peninsula, with an associated rainfall change involving the intensification of ITCZ over a broad region encompassing the African and Indian continents.

Otherwise, one can also note some obvious differences between the anomalous circulation responses in Fig. 9c (as connected to ISM rainfall intensification) and Fig. 9a (as associated with the enhanced AMTG), especially over the Indian Ocean. Although both figures show anomalous anticyclonic easterlies over north-west Pacific which also promotes convergence of low-level circulation to Indian landmass, these are slightly more pronounced in Fig. 9c than in Fig. 9a. The other notable difference includes, while Fig 9a show the gigantic low extending all the way from Sahara to Arabian region, it is considerably weaker and somewhat restricted to Arabia in Fig 9c.

5. Summary and concluding remarks

In the backdrop of the earlier studies suggesting large inter-model spread in ISM rainfall projections under high-emission scenarios (e.g., Sooraj et al 2015; 2016; IPCC 2013, 2021), the current study analyzed the CMIP6 projections (SSP585) to bring more clarity on two aspects: (a). what are the main physical processes associated with the ÍSM rainfall enhancements in future projections using the last generation of CMIP models; (b) what are the sources of uncertainty in the projected ISM rainfall thus enabling us to unravel the underlying factors.

Firstly, the insights from moisture budget analyses, based on the MME, show that both the TH and DY components are instrumental in enhancing ISM rainfall in the SSP585

projections, with the former one assuming a dominant role. The dominating role of TH follows the Clausius-Clapeyron equation with the increased water-holding capacity of the atmosphere under global warming (Held and Soden 2006; Cherchi et al 2011; Li and Ting 2017; Jiang et al 2023). However, an important inference from this study is that both the TH and DY components show complementary effects in CMIP6 MME projections thus eventually contributing to the ISM rainfall enhancements which is in contrast with the pronounced offsetting behaviour in its earlier versions (i.e., CMIP5 MME). In other words, the dominant drying effect of DY term, as observed across the CMIP5 models (Chen and Zhou 2015; Sooraj et al 2015, 2016), has transitioned to prominent wetting effect in CMIP6 MME. However, the drying and wetting changes due to DY term is not uniform across the CMIP6 models thus explaining its large inter-model spread. It is further inferred that the DY component dominantly account for the model's uncertainty ISM rainfall projections with a secondary contribution from the TH. Coinciding with this, there is a large inter-model spread both in lower and upper tropospheric circulations, with both the low and upper-level signatures (i.e., strengthening and weakening) demonstrating strong coupling across the models.

The second part of our study illustrated the possible drivers of model's uncertainty in future ISM rainfall projections. Previous studies on the ISM rainfall projections are primarily focussed on the inter-model spread in the global warming rate (i.e., global mean temperature, GMT) thus partially accounting for the projected uncertainties (Chen and Zhou 2015; Chen et al 2020). The current study also confirms the same, the interhemispheric TS contrast (IHTG), as found to be linked physically to GMT and ECS, is one of the important sources of uncertainty in the future ISM rainfall projections. The DY component is in-turn found to be significantly associate with both ECS and GMT, implying strong sensitivity of DY term to ECS, i.e., models with a higher ECS (or GMT) incline to project a stronger DY. Thus, it is inferred that the inter-model spread in DY term account for the ISM rainfall uncertainty as partially driven by IHTG

through the interhemispheric energy transport which controls the migration of ITCZ towards the warmer hemisphere as demonstrated in several studies (e.g., Schneider et al 2014; Byrne et al. 2018; Biasutti et al 2018). However, surprisingly, TH shows no sensitivity to GMT which looks counter-intuitive as contradicting the expected hypothetical Clausius-Clapeyron scaling (e.g., Held and Soden 2006; Chou et al 2009; Chou et al 2012; Cherchi et al 2011; Huang 2014; Chen and Zhou 2015; Jiang et al 2023).

Considering the prominent inter-model diversity in ECS (Forster et al 2021; Hausfather et al 2022), we further incorporated the GMT scaling to account for the large variation of GMT across the models. Interestingly, by applying the GMT scaling, it reveals an entirely different picture with no clear interhemispheric TS signatures (IHTG). Instead, the inter-model spread in DY and ISM rainfall changes are prominently driven by meridional TS signatures over the Atlantic (AMTG) thus bringing the importance of divergent Atlantic warming pattern across the models as an emerging factor accounting for the projected uncertainty in ISM rainfall. The interpretation is that a larger projected increase of AMTG leads to a stronger low-level cross equatorial moisture transport through intensification of regional Low extending from the Sahara to Arabian Peninsula thus increasing the Sahelian-Indian monsoon rainfall in the future projections which follows the inferences drawn in earlier studies as well (e.g., Liu et al 2014; Vital et al 2020; Yang and Huang 2021; Zhang and Li 2022; Sooraj et al 2023; Terray et al 2023).

The state-of-the-art coupled models are known to suffer from systematic biases over the tropics in particular over the ISM regions and Atlantic Ocean (e.g., Sperber et al 2013; Richter et al 2014; Sooraj et al 2015, 2016; Terray et al 2018, 2023; Choudhury et al 2021; Rajendran et al 2022; Zhang and Li 2022). So, these biases may have large implications in truly representing the monsoon characteristics in future projections and hence may also play a role in determining the projected rainfall uncertainty. One of the prominent systematic errors in

CMIP5 and CMIP6 simulations as relevant to ISM is the prominent dry bias which remains still unresolved (e.g., Sperber et al 2013; Sooraj et al 2015, 2016; Terray et al 2018; Choudhury et al 2021; Rajendran et al 2022). Furthermore, the systematic rainfall errors from the CMIP6 models show wet biases over southwest Arabian Sea (see Fig 10), thus demonstrating a systematic dry-wet pattern (i.e., dry bias over Indian landmass and wet bias over Oceanic regions to the south of it), which persists in many climate models and are coupled to Indian Ocean SST biases (Bollasina and Ming 2013; Prodhomme et al 2014; Annamalai et al 2017; Terray et al 2021). Recently, Choudhury et al (2021) also inferred similar dry-wet pattern while assessing the fidelity of CMIP6 models in representing ISM rainfall climatology (using its historical simulations) which they attributed to the persistent simulation of the continental ITCZ to a southward location (at 12°N) by most of the CMIP6 models. Earlier we noted anomalous westward extension of rainfall in the future projections as characterised by rainfall intensification over the southwest Arabian Sea, intriguingly coinciding with the same region showing a prominent wet bias in current climate models, as stated above. These results raise relevant questions on the mutual linkages between future rainfall changes (Fig 1a) and coupled biases (Fig 10c) which needs to be further explored in order to reduce the model's uncertainties. However, the detailed role of coupled model biases on ISM rainfall future projections is beyond the scope of this study. Our future works will be focused in this direction to apply observational constraints on future ISM rainfall projections.

Acknowledgments

We sincerely thank Dr. R. Krishnan, Director, Indian Institute of Tropical Meteorology (IITM, India) and Dr. J. Sanjay, Project Director, Centre for Climate Change Research (CCCR at IITM) for all the support during the research study. Ajinkya M. Aswale and Sooraj K P are funded by the CCCR and IITM, which are fully funded by the Ministry of Earth Sciences, Government of India. Pascal Terray is funded by Institut de Recherche pour le Développement (IRD, France).

References

Abish, B., P. V. Joseph, O. M. Johannessen, 2013: Weakening Trend of the Tropical Easterly Jet Stream of the Boreal Summer Monsoon Season 1950–2009. *J. Climate*, **26**, 9408–9414, https://doi.org/10.1175/JCLI-D-13-00440.1.

Annamalai H, Taguchi B, McCreary JP, Nagura M, Miyama T (2017) Systematic errors in South Asian monsoon simulation: importance of equatorial Indian Ocean processes. J Clim 30, 8159-8178.

Ashrit RG, Kitoh A, Yukimoto S (2005) Transient response of ENSO—monsoon teleconnection in MRI-CGCM2.2 climate change simulations. J Meteorol Soc Jpn 83:273–291

Bretherton CS, Sobel AH (2002) A simple model of a convectively-coupled Walker circulation using the weak temperature gradient approximation. J. Clim. 15:2907–20

Biasutti M, et al (2018) Global energetics and local physics as drivers of past, present and future monsoons. Nat. Geosci., 11, 392–400, https://doi.org/10.1038/s41561-018-0137-1.

Bollasina, M.A., Ming, Y. (2013) The general circulation model precipitation bias over the southwestern equatorial Indian Ocean and its implications for simulating the South Asian monsoon. Clim Dyn 40, 823–838.

Byrne, M. P., A. G. Pendergrass, A. D. Rapp, K. R. Wodzicki (2018) Response of the intertropical convergence zone to climate change: Location, width, and strength. Curr. Climate Change Rep., 4, 355–370, https://doi.org/10.1007/s40641-018-0110-5.

Chen, X., T. Zhou (2015), Distinct effects of global mean warming and regional sea surface warming pattern on projected uncertainty in the South Asian summer monsoon, Geophys. Res. Lett., 42, 9433–9439, doi:10.1002/2015GL066384.

Chen, Z., Zhou, T., Zhang, L., Chen, X., Zhang, W., Jiang, J. (2020). Global land monsoon precipitation changes in CMIP6 projections. Geophysical Research Letters, 47, e2019GL086902. https://doi.org/10.1029/2019GL086902

Chen, Z., Zhou, T., Chen, X. *et al.* (2022) Observationally constrained projection of Afro-Asian monsoon precipitation. *Nat Commun* **13**, 2552. https://doi.org/10.1038/s41467-022-30106-z

Chen, YJ., Hwang, YT., Lu, J. (2024a) Robust increase in South Asian monsoon rainfall under warming driven by extratropical clouds and ocean. *npj Clim Atmos Sci* **7**, 318 (2024). https://doi.org/10.1038/s41612-024-00843-7

Chen, Z., T. Zhou, X. Chen, L. Zhang, Y. Qian, Z. Wang, L. He, L. R. Leung, (2024b) Understanding the Biases in Global Monsoon Simulations from the Perspective of Atmospheric Energy Transport. *J. Climate*, **37**, 4647–4666, https://doi.org/10.1175/JCLI-D-23-0444.1.

Cherchi A, Alessandri, A., Masina, S., Navarra, A (2011) Effects of increased CO2 levels on monsoons. Clim. Dyn. 37, 83–101.

Chou, C., J. D. Neelin, C.-A. Chen, J.-Y. Tu (2009) Evaluating the "Rich-Get-Richer" Mechanism in Tropical Precipitation Change under Global Warming. Journal of Climate, 22, 1982-2005. https://doi.org/10.1175/2008jcli2471.1.

Chou C, Chen CA, Tan PH, Chen KT (2012) Mechanisms for global warming impacts on precipitation frequency and intensity. J Clim 25:3291–3306

Dai A, et al. (2013) The relative roles of upper and lower tropospheric thermal contrasts and tropical influences in driving Asian summer monsoons. J. Geophys. Res. Atmos. 118, 7024–7045.

Douville H, Raghavan K, Renwick J, et al (2021) Water cycle changes, Chap 8. Intergovernmental panel for climate change (IPCC), Working group 1 (WG1), Sixth assessment report (AR6)

Endo H, Kitoh A (2014) Thermodynamic and dynamic effects on regional monsoon rainfall changes in a warmer climate. Geophys. Res. Lett. 41, 1704–1710

Endo H, Kitoh A, Ueda H (2018) A unique feature of the Asian summer monsoon response to global warming: the role of different land–sea thermal contrast change between the lower and upper troposphere. Sci. Online Lett. Atmos. 14, 57–63. doi: 10.2151/sola.2018-010.

Eyring V, Bony S, Meehl GA, et al (2016) Overview of the Coupled Model Intercomparison Project Phase 6 (CMIP6) experimental design and organization. Geosci Model Dev 9:1937–1958

Forster P M, et al (2013) Evaluating adjusted forcing and model spread for historical and future scenarios in the CMIP5 generation of climate models. J. Geophys. Res. Atmos. 118, 1139–1150.

Forster, P., Storelvmo, T., Armour, K., Collins, W., Dufresne, J.-L., Frame, D., et al. (2021). The Earth's energy budget, climate feedbacks, and climate sensitivity. In V. Masson-Delmotte, P. Zhai, A. Pirani, S. L. Connors, C. Pean, S. Berger, et al. (Eds.), Climate change 2021: The physical science basis. Contribution of working group I to the sixth assessment report of the intergovernmental panel on climate change (pp. 923–1054). Cambridge University Press. https://doi.org/10.1017/9781009157896.009

Gregory J M et al (2004) A new method for diagnosing radiative forcing and climate sensitivity. Geophys. Res. Lett. 31, https://doi.org/10.1029/2003gl018747.

Guilbert M, P Terray, J Mignot (2023) Intermodel spread of historical Indian monsoon rainfall change in CMIP6: The role of the tropical Pacific mean-state. J. Climate, 36, 3937–3953, https://doi.org/10.1175/JCLI-D-22-0585.1.

Guilbert, M., P. Terray, J. Mignot, L. Ollier, G. Gastineau (2024) Interhemispheric Temperature Gradient and Equatorial Pacific SSTs Drive Sahel Monsoon Uncertainties under Global Warming. J. Climate, 37, 1033–1052, https://doi.org/10.1175/JCLI-D-23-0162.1.

Hausfather Z, Marvel K, Schmidt G A, Nielsen-Gammon J W, Zelinka M (2022). Climate simulations: Recognize the 'hot model' problem. Nature, 605(7908), 26–29. https://doi.org/10.1038/d41586-022-01192-2

Hawkins E, Sutton R (2009) The Potential to narrow uncertainty in regional climate predictions. Bull. Am. Meteorol. Soc. 90, 1095–1108.

Held I M, Soden B J (2006) Robust responses of the hydrological cycle to global warming. J. Clim. 19, 5686–5699.

Huang P (2014) Regional response of annual-mean tropical rainfall to global warming. Atmos. Sci. Lett., 15, 103–109, doi:10.1002/asl2.475.

Huang P, Xie S-P, Hu K, Huang G, Huang R (2013) Patterns of the seasonal response of tropical rainfall to global warming. Nat. Geosci., 6, 357–361

IPCC (2001) Third assessment report of the intergovernmental panel on climate change. www.ipcc.ch/ipccreports/ar4-wg1.htm

IPCC (2007) Fourth assessment report of the intergovernmental panel on climate change. www.ipcc.ch/ipccreports/ar4-wg1.htm

IPCC (2013) Fifth assessment report of the intergovernmental panel on climate change. www.ipcc.ch/ipccreports/ar4-wg1.htm

IPCC (2021) Intergovernmental Panel on Climate Change Sixth Assessment Report. The IPCC Scientific Assessment.

Jiang Y, Zhu Z, Li J, Miao L, Miao Z (2023) Changes of mean and extreme precipitation and their relationship in Northern Hemisphere land monsoon domain under global warming. Int. J. Climatol. 43, 5536–5552.

Jin et al (2020) Future Changes and Controlling Factors of the Eight Regional Monsoons Projected by CMIP6 Models, DOI: 10.1175/JCLI-D-20-0236.1

Kitoh A, Yukimoto S, Noda A, Motoi T (1997) Simulated changes in the Asian summer monsoon at times of increased atmospheric CO2. J Meteorol Soc Jpn 75:1019–1031

Kitoh et al. et al., (2013) Monsoons in a changing world: A regional perspective in a global context. Journal of Geophysical Research: Atmospheres, 118(8), 3053–3065, doi:10.1002/jgrd.50258

Kulkarni, A. et al., (2020) Precipitation Changes in India. In: Assessment of Climate Change over the Indian Region: A Report of the Ministry of Earth Sciences (MoES), Government of India

[Krishnan, R., J. Sanjay, C. Gnanaseelan, M. Mujumdar, A. Kulkarni, and S. Chakraborty (eds.)]. Springer Singapore, Singapore, pp. 47–72, doi:10.1007/978-981-15-4327-2_3.

Lehner F, Deser C, Maher N, Marotzke J, Fischer E M, Brunner L, et al. (2020) Partitioning climate projection uncertainty with multiple large ensembles and CMIP5/6. Earth System Dynamics, 11(2), 491–508. https://doi.org/10.5194/esd-11-491-2020

Li X, Ting M (2017) Understanding the asian summer monsoon response to greenhouse warming: the relative roles of direct radiative forcing and sea surface temperature change. Clim Dyn 2017; 49: 2863-2880. https://doi.org/10.1007/s00382-016-3470-3

Li G, Xie S-P, He C, Chen Z (2017) Western pacific emergent constraint lowers projected increase in Indian summer monsoon rainfall. *Nature Climate Change*, *7*(10), 708–712

Li T, et al (2022) Distinctive South and East Asian monsoon circulation responses to global warming. Sci. Bull. 67, 762–770

Liu Y, Chiang JCH, Chou C, Patricola CM (2014) Atmospheric teleconnection mechanisms of extratropical North Atlantic SST influence on Sahel rainfall. Clim Dyn 43:2797–2811

Long S M, Li G (2021) Model Uncertainty in the Projected Indian Summer Monsoon Precipitation Change under Low-Emission Scenarios. Atmosphere, 12, 248. https://doi.org/10.3390/atmos12020248

Long S.-M., Xie S.-P., Liu W (2016) Uncertainty in tropical rainfall projections: Atmospheric circulation effect and the Ocean Coupling. J. Clim., 29, 2671–2687.

Luo, H., Wang, Z., He, C. *et al.* (2024) Future changes in South Asian summer monsoon circulation under global warming: role of the Tibetan Plateau latent heating. *npj Clim Atmos Sci* **7**, 103. https://doi.org/10.1038/s41612-024-00653-x

Ma J, Yu JY. (2014) Paradox in South Asian summermonsoon circulation change: lower tropospheric strengthening and upper tropospheric weakening. Geophys. Res. Lett. 41:2934–40

Ma, J., Xie, S. P. & Kosaka, Y. (2012) Mechanisms for tropical tropospheric circulation change in response to global warming. J. Clim. 25, 2979–2994

Ma, J., Chadwick, R., Seo, K.-H., Dong, C., Huang, G., Foltz, G. R., and Jiang, J. H. (2018). Responses of the tropical atmospheric circulation to climate change and connection to the hydrological cycle. Annual Review of Earth and Planetary Sciences, 46 :549–580.

May W (2002). Simulated changes of the Indian summer monsoon under enhanced greenhouse gas conditions in a global time-slice experiment. Geophys. Res. Lett. 29, 1118.

May, W., (2004) Potential future changes in the Indian summer monsoon due to greenhouse warming: Analysis of mechanisms in a global time-slice experiment. Climate Dyn., 22, 389–414, https://doi.org/10.1007/s00382-003-0389-2

May, W. (2011) The sensitivity of the Indian summer monsoon to a global warming of 2_C with respect to pre-industrial times. Clim. Dyn. 37, 1843–1868.

Meehl, G. A. et al. (2020) Context for interpreting equilibrium climate sensitivity and transient climate response from the CMIP6 Earth system models. Sci. Adv. 6, eaba1981.

Menon et al., (2013) Consistent increase in Indian monsoon rainfall and its variability Geoscientific across CMIP-5 models., 287–300, doi:10.5194/esd-4-287-2013

Monerie, P.-A., E. Sanchez-Gomez, B. Pohl, J. Robson, and B.Dong (2017) Impact of internal variability on projections of Sahel recipitation change. Environ. Res. Lett., 12, 114003, https://doi.org/10.1088/1748-9326/aa8cda

O'Neill BC, Tebaldi C, Van Vuuren DP, et al (2016) The scenario model intercomparison project (ScenarioMIP) for CMIP6. Geosci Model Dev 9:3461–3482

Paula JB, Kummerow CD (2014) An assessment of atmospheric water budget components over tropical oceans. J Clim 27:2054–2071

Prodhomme, C., Terray, P., Masson, S. et al. (2014) Impacts of Indian Ocean SST biases on the Indian Monsoon: as simulated in a global coupled model. Clim Dyn 42, 271-290.

Rajesh, P. V., and Goswami, B. N. (2022) A new emergent constraint corrected projections of Indian summer monsoon rainfall. Geophysical Research Letters, 49, e2021GL096671. https://doi.org/10.1029/2021GL096671

Richter I, Xie S-P, Behera S, Doi T, Masumoto Y (2014) Equatorial Atlantic variability and its relation to mean state biases in CMIP5. Clim Dyn 42:171. https://doi.org/10.1007/s00382-012-1624-5

Schneider, T., T. Bischoff, and G. H. Haug, (2014) Migrations and dynamics of the intertropical convergence zone. Nature, 513, 45–53, https://doi.org/10.1038/nature13636.

Seager, R.; Naik, N.; Vecchi, G.A. (2010) Thermodynamic and dynamic mechanisms for large-scale changes in the hydrological cycle in response to global warming. J. Clim. 23, 4651–4668

Sharmila et al. (2015) Future projection of Indian summer monsoon variability under climate change scenario: An assessment from CMIP5 climate models. Global and Planetary Change, 124, 62–78, doi:10.1016/j.gloplacha.2014.11.004.

Sooraj et al., (2015) Global warming and the weakening of the Asian summer monsoon circulation: assessments from the CMIP5 models. Climate Dynamics, 45(1–2), 233–252, doi:10.1007/s00382-014-2257-7.

Sooraj, K.P., Terray, P., Masson, S., Cretat, J., (2019) Modulations of the Indian summer monsoon by the hot subtropical deserts: insights from coupled sensitivity experiments. Climate Dynamics. 52, 4527–4555. https://doi.org/10.1007/s00382-018-4396-8.

Sooraj, K.P., Terray, P., Shilin, A., Mujumdar, M., (2020) Dynamics of rainfall extremes over India: A new perspective. International Journal of Climatology. 10.1002/joc.6516.

Sooraj KP, Aswale AM, Swapna P, et al (2023) Modulations in the Indian Summer Monsoon–ENSO teleconnections by the North Tropical Atlantic. Clim Dyn 1–20

Srivastava AK, DelSole T (2014) Robust forced response in South Asian summer monsoon in a future climate. J Clim 27:7849–7860

Storch HV, Zwiers FW (2002) Statistical analysis in climate research. Cambridge University Press, UK, p 494

Sun, Y., Ding, Y., Dai, A. (2010) Changing links between South Asian summer monsoon circulation and tropospheric land-sea thermal contrasts under a warming scenario. Geophys. Res. Lett. 37, L02704.

Terray, P., Sooraj, K.P., Masson, S., Krishna, R.P.M., Samson, G., Prajeesh, A.G., (2018) Towards a realistic simulation of boreal summer tropical rainfall climatology in state-of the-art climate coupled models. Clim Dyn. 50, 3413–3439 doi:10.1007/s00382-017-3812-9

Terray, P., K.P. Sooraj, S. Masson, C. Prodhomme (2021) Anatomy of the Indian Summer Monsoon and ENSO relationships in state-of-the-art CGCMs: Role of the tropical Indian Ocean, Climate Dynamics., Vol. 56: 329–356

Terray P, Joseph L, Sooraj KP (2023) Anatomy of the Indian summer monsoon and ENSO relationship in a state-of-the-art CGCM: role of the tropical Atlantic Ocean. Clim Dyn 60:1559–1582

Ueda, H.; Iwai, A.; Kuwako, K.; Hori, M.E. (2006) Impact of anthropogenic forcing on the Asian summer monsoon as simulated by eight GCMs. Geophys. Res. Lett., 33, L06703

Vittal H, Villarini G, Zhang W (2020) Early prediction of the Indian summer monsoon rainfall by the Atlantic Meridional Mode. Clim Dyn 54:2337–2346. https://doi.org/10.1007/s00382-019-05117-0

Wang, Bin., & Qinghua, Ding (2006). Changes in Global Monsoon Precipitation over the Past 56 Years. *Geophysical Research Letters* 33, no. 6.

Webster PJ, Magana VO, Palmer TN, Shukla J, Tomas RA, Yanai MU, et al (1998). Monsoons: Processes, predictability, and the prospects for prediction. J Geophys Res.103(C7):14451–510.

Williamson, M. S., Cox, P. M., Huntingford, C., & Nijsse, F. J. (2024). Testing the assumptions in emergent constraints: why does the “emergent constraint on equilibrium climate sensitivity

from global temperature variability" work for CMIP5 and not CMIP6?. Earth System Dynamics, 15(4), 829-852.

Wilson SS, Joseph PV, Mohanakumar K & Ola M. Johannessen (2018) Interannual and long term variability of low level jetstream of the Asian summer monsoon, Tellus A: Dynamic Meteorology and Oceanography, 70:1, 1-9, DOI:10.1080/16000870.2018.1445380

Wu, Q. et al. (2022) Asian summer monsoon responses to the change of land–sea thermodynamic contrast in a warming climate: CMIP6 projections. Adv. Clim. Chang. Res. 13, 205–217.

Xie, S.-P.; Deser, C.; Vecchi, G.A.; Collins, M.; Delworth, T.L.; Hall, A.; Hawkins, E.; Johnson, N.C.; Cassou, C.; Giannini, A.; et al (2015) Towards predictive understanding of regional climate change. Nat. Clim. Chang. 5, 921–930.

Yang X, Huang P (2021) Restored relationship between ENSO and Indian summer monsoon rainfall around 1999/2000. The Innovation 2:100102. https://doi.org/10.1016/j.xinn.2021.100102

Zhang, Z., and G. Li, (2022) Uncertainty in the projected changes of Sahel summer rainfall under global warming in CMIP5 and CMIP6 multi-model ensembles. Climate Dyn., 59, 3579–3597, https://doi.org/10.1007/s00382-022-06284-3

Zhou, T., Lu, J., Zhang, W., & Chen, Z. (2020). The sources of uncertainty in the projection of global land monsoon precipitation. Geophysical Research Letters, 47, e2020GL088415. https://doi.org/10.1029/2020GL088415

Main Figures

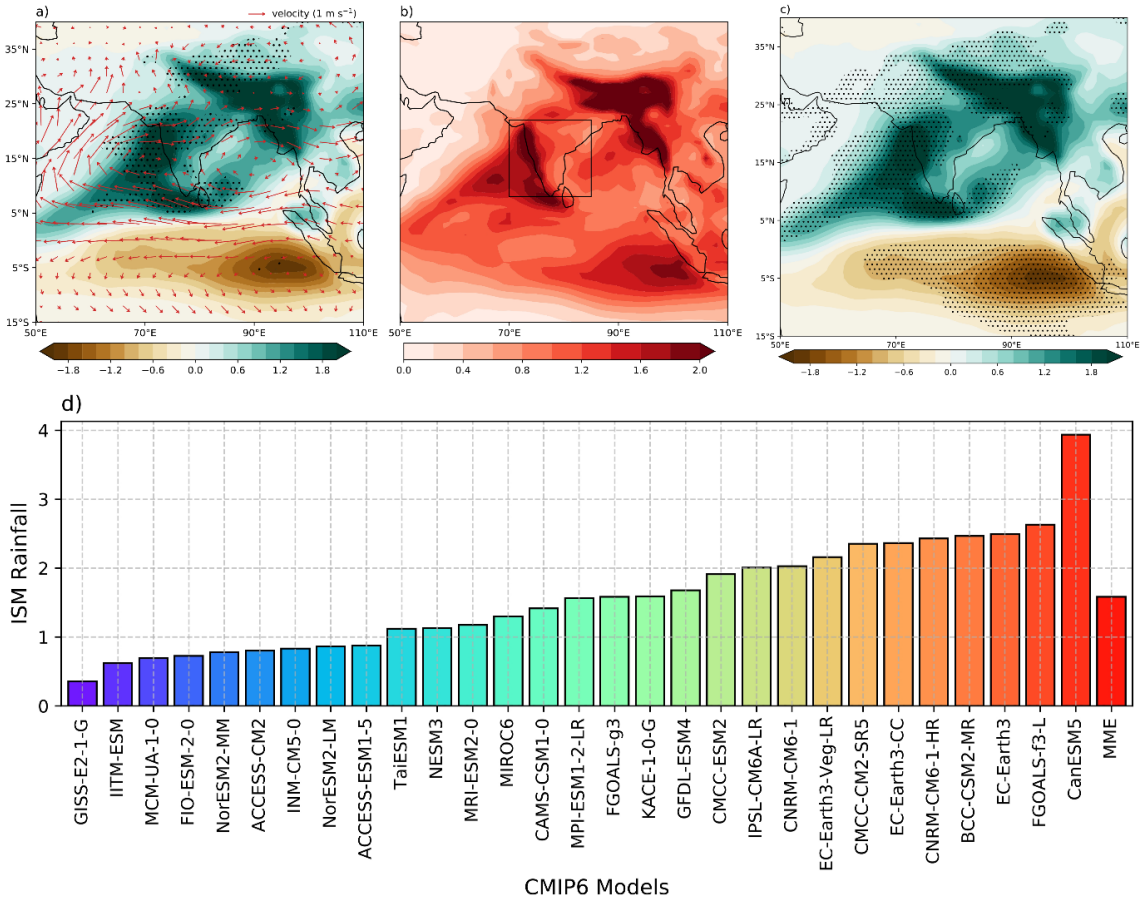


Fig 1:) Future change in JJAS Climatology of (a) rainfall for MME of 30 models with over laying wind at 850hPa level. Historical simulations are for 1979-2013 and high emission scenario SSP585 are for 2065-2099. Difference between future and historical (i.e., future minus historical) represents the future change. Dotted region in (a) represents where the future changes exceed well above the signal to noise ratio (SNR). SNR is defined as (see Section 2) the MME divided by its inter-model standard deviation (SD). In (b), inter-model SD in future rainfall change. In (c), same as (a), but the dotted regions represent significant future change based on 90% level of significance using a two-tailed Student's t-test. The units are mm/day for rainfall and m/s for wind. In (d), future change in rainfall as averaged over Indian region containing both land and ocean grid points (i.e., ISM rainfall over 70°E-85°E, 8°N-22°N, in mm/day) for all 30 models.

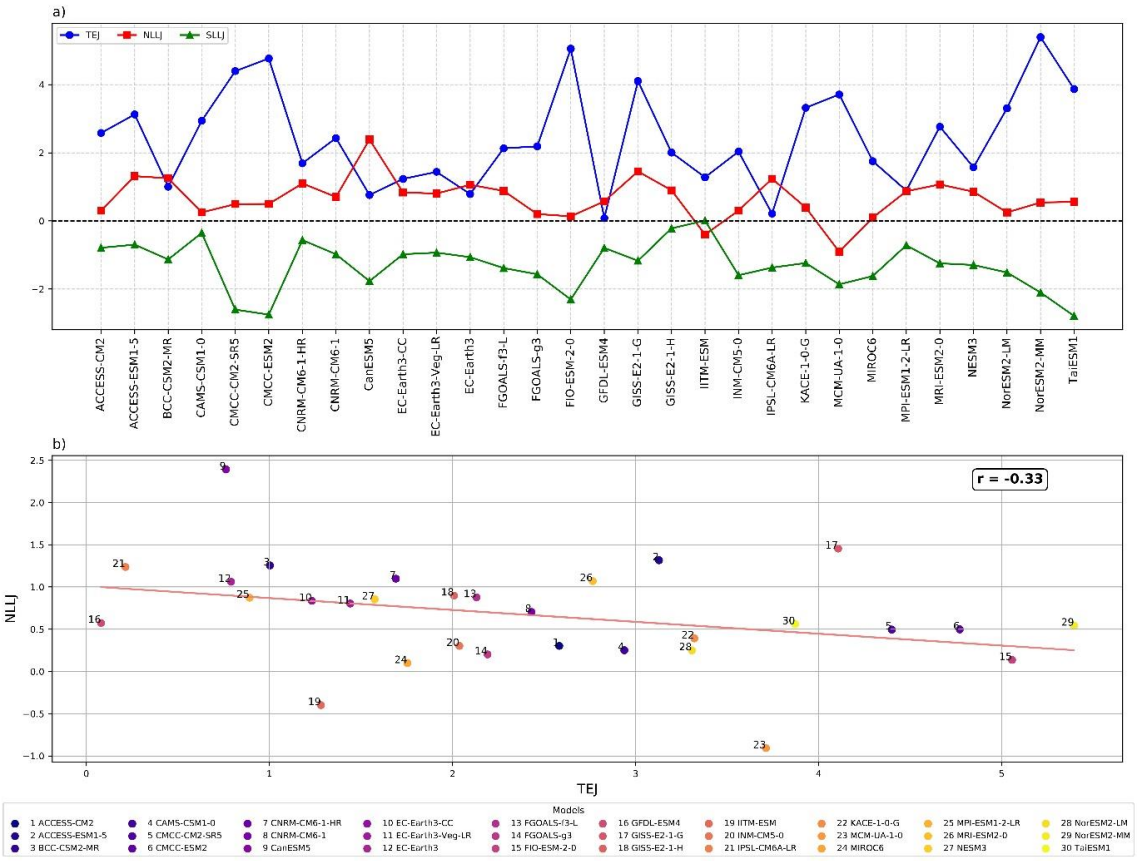


Fig 2: In (a), future change in atmospheric circulation indices (see Table 2) for all 30 models. Here, NLLJ index refers to 850hPa zonal wind as averaged over Arabian region (over 55°E-65°E, 10°N-20°N), while SLLJ index denotes 850hPa zonal wind averaged over 55°E-65°E, Eq-10°N. TEJ index stands for 200 hPa zonal wind as averaged over 40°E-100°E, 10°S-20°N. In (b), scatter plot between NLLJ and TEJ. Units are in m/s.

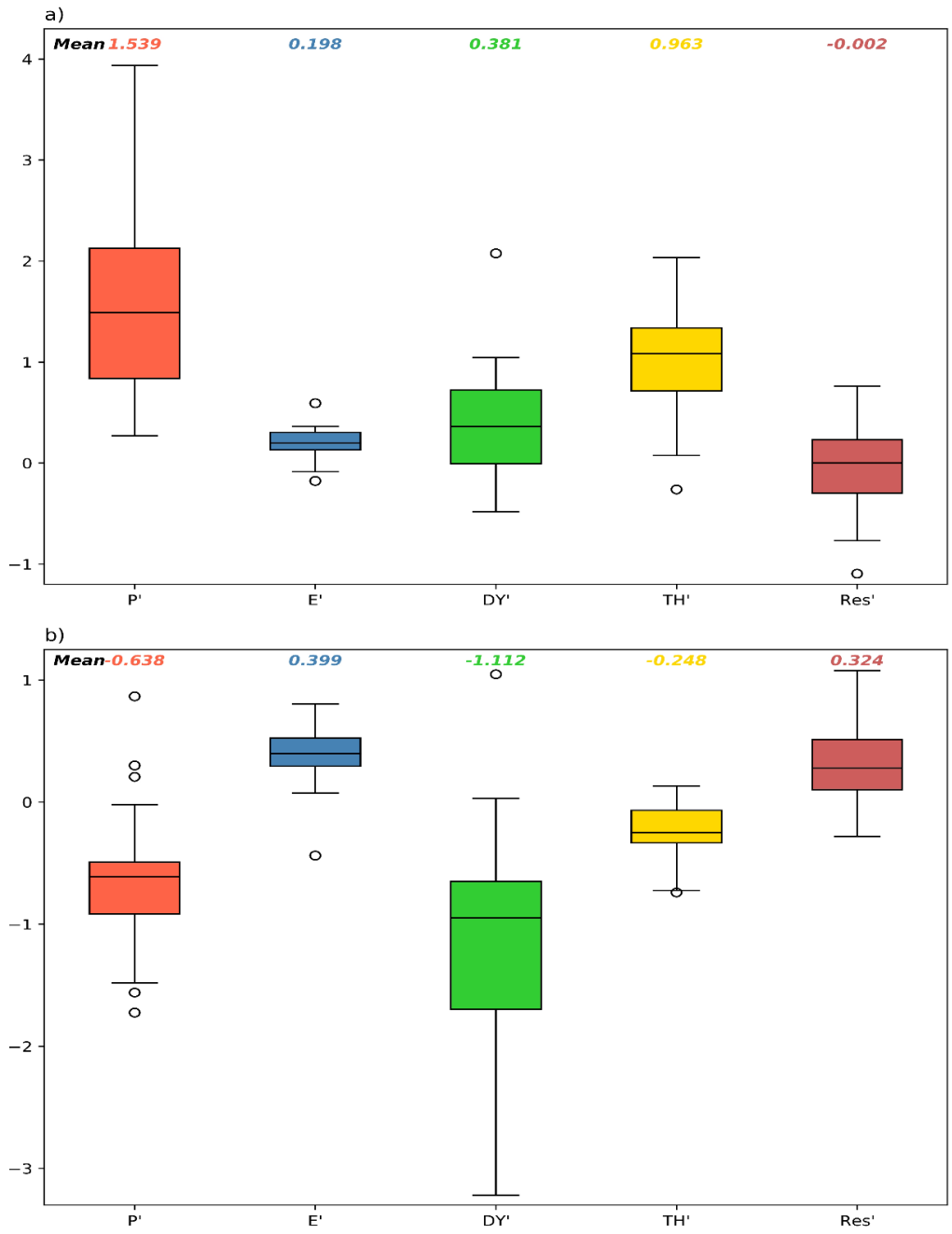


Fig 3: (a) Box and whisker plots showing the future changes in moisture budget terms (using Equations (2 and 3)) as averaged over the ISM domain (70°E-85°E, 8°N-22°N). The whiskers outside the box represents the inter-model spread, while the boxes indicate the interquartile range with the mean (MME) represented by the horizontal line inside the box. P' stands for ISM rainfall changes, E' is for evaporation changes, DY' is for changes in dynamic component, TH' is for changes in thermodynamic component and RES' represent the Residual changes as calculated based on moisture budget over ISM region. In (b), same as (a), but for the changes in moisture budget terms over the south-east Indian Ocean region (20°S-Equator, 70°E-100°E). Units are in mm/day for all the budget terms.

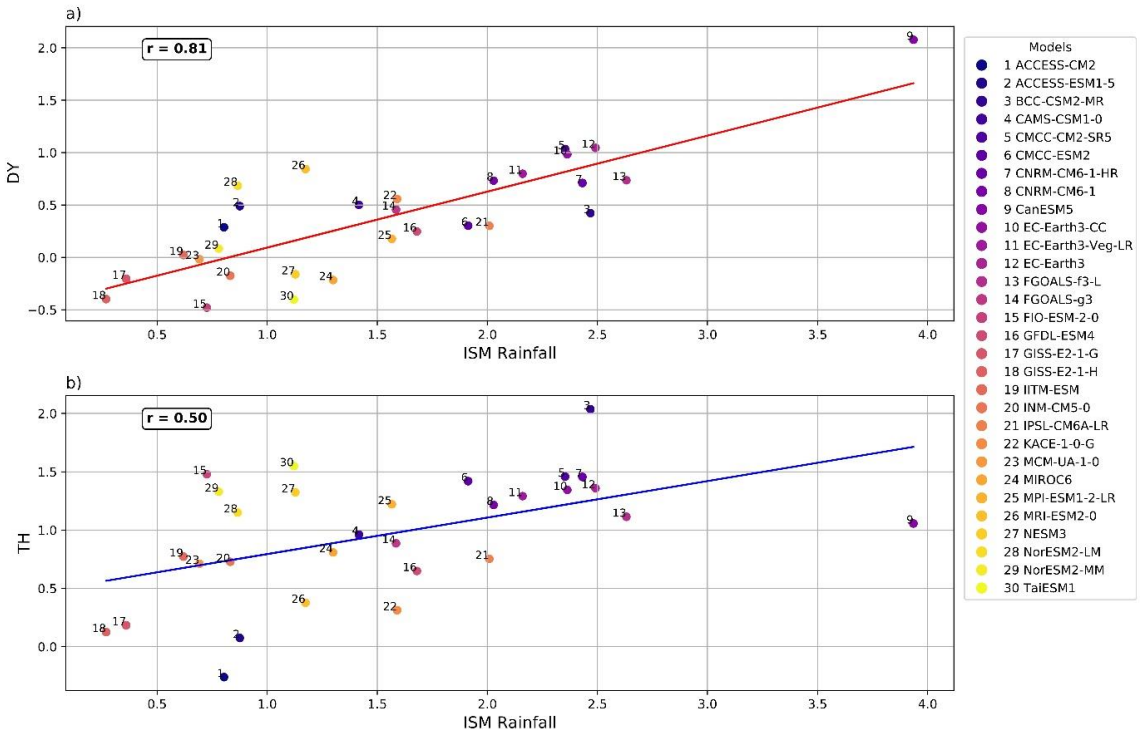


Fig 4: a) Scatter plots between ISM rainfall change (over 70°E-85°E, 8°N-22°N, mm/day) and Dynamic component (DY averaged over ISM region, mm/day), using all 30 models. In (b), same as (a), but between ISM rainfall change (over 70°E-85°E, 8°N-22°N, mm/day) and Thermodynamic component (TH averaged over ISM region).

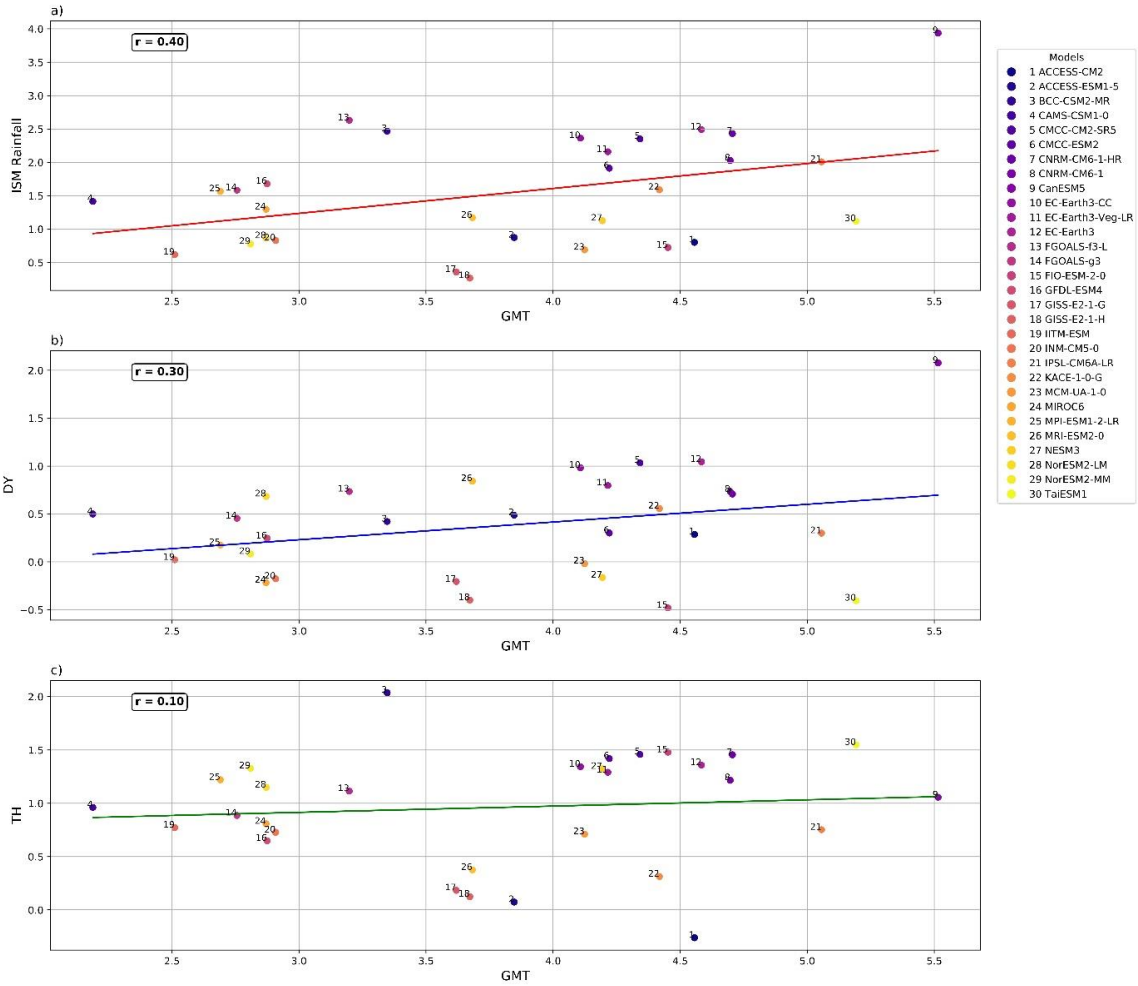


Fig 5: In (a): scatter plot between future changes in Global Mean Temperature (GMT, °C) change and ISM rainfall (i.e., over 70°E-85°E, 8°N-22°N, mm/day). In (b), same as (a), but between GMT change and Dynamic component (DY averaged over ISM region, mm/day). In (c), same as (a), but between GMT change and Thermodynamic component (TH averaged over ISM region, mm/day).

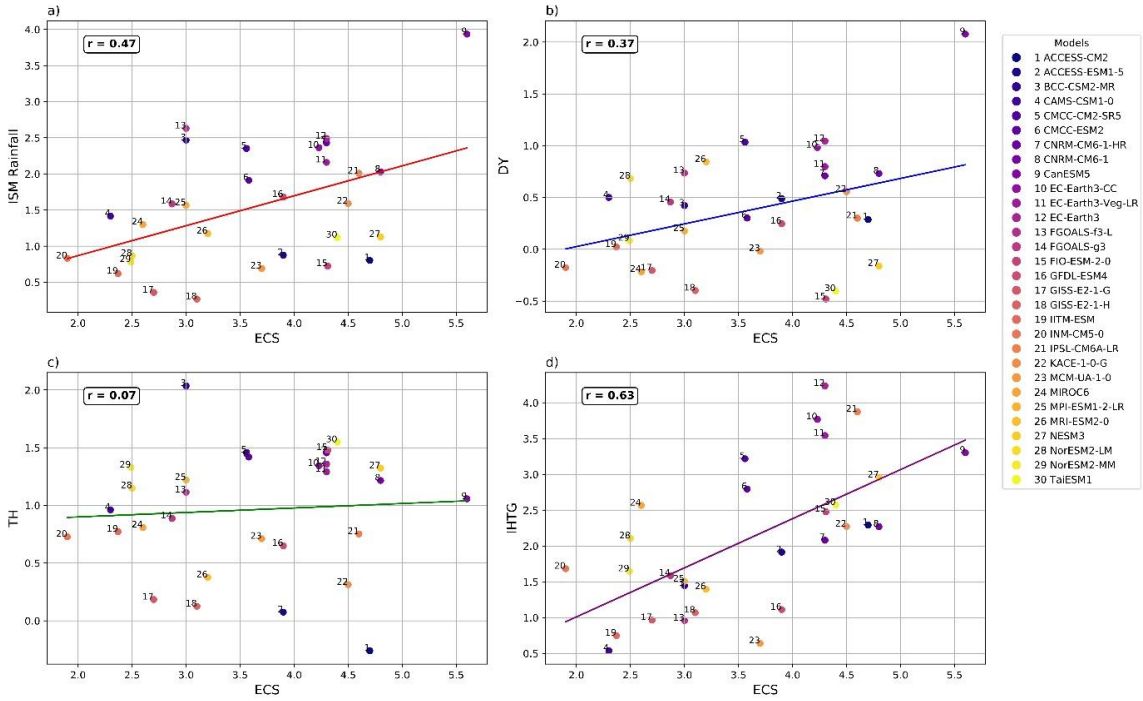


Fig 6: In (a): scatter plot between Equilibrium Climate Sensitivity (ECS, °C) and ISM rainfall change (i.e., over 70°E-85°E, 8°N-22°N, mm/day). In (b), same as (a), but between ECS and Dynamic component (DY over ISM, mm/day). In (c), same as (a), but between ECS and Thermodynamic component (TH over ISM, mm/day). In (d), scatter plot between ECS (°C) and IHTG (interhemispheric TS gradient, °C). As per Section 2, the IHTG is defined as the difference between TS averaged over the region to the north (i.e., over 25°N to 90°N and 0° to 360°E) and south (i.e., over 60°S to 25°N and 0° to 360°E) of 25°N. Note that in (d), the GMT is subtracted from the TS change at every grid point for each model subtracted at every grid point for each model before computing the IHTG.

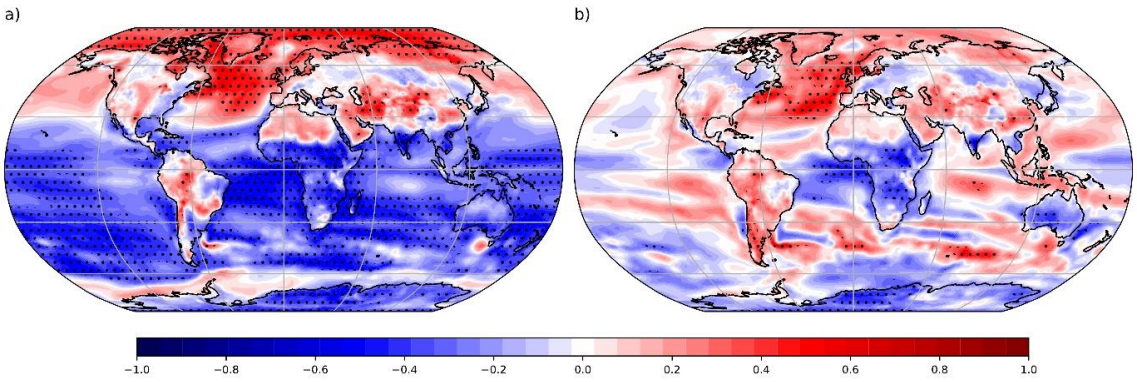


Fig 7: In (a), inter-model correlation analysis between future ISM rainfall Index and TS future change. Correlations significant at the 90% confidence level are marked with dots. Note that in (a), the GMT change is subtracted from the TS change at every grid point for each model before doing the inter-model correlation analysis. In (b), same as (a), but after scaling by GMT, i.e., both ISM rainfall index and TS changes are scaled using GMT changes (divided by GMT) of each model.

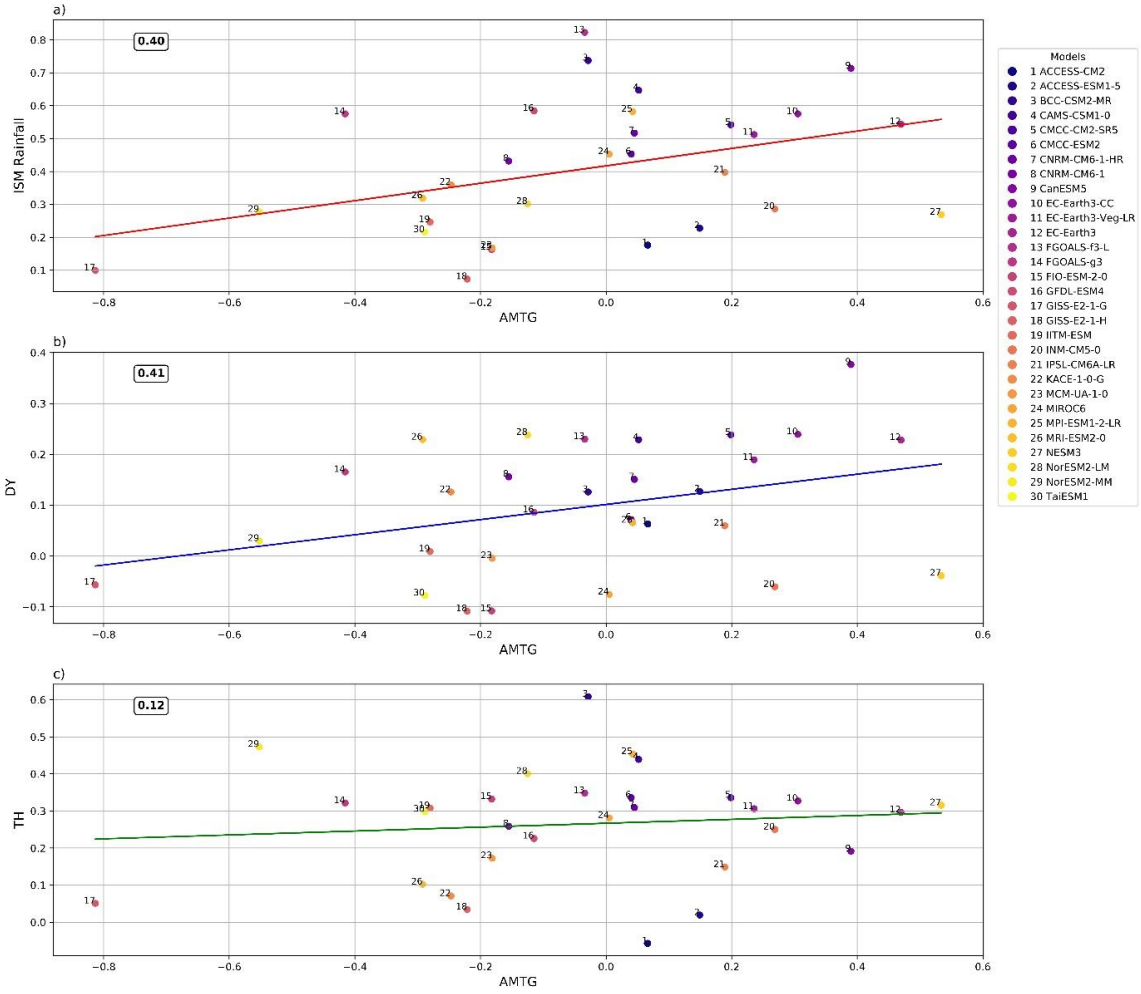


Figure 8: In (a), scatter plot but between the future changes in Atlantic Meridional Temperature Gradient (AMTG) Index and ISM rainfall. In (b), same as (a), but between AMTG and DY component. In (c), same as (b), but DY is replaced with TH. Atlantic meridional TS gradient (AMTG) is defined as North Atlantic TS over 40°W-10°W, 25°N-65°N minus South Atlantic TS over 40°W-10°W, 25°S-5°N. DY and TH are averaged over ISM region (i.e. over 70°E-85°E, 8°N-22°N). Note that all the variables are scaled by GMT (divided by GMT) of each model before the calculation.

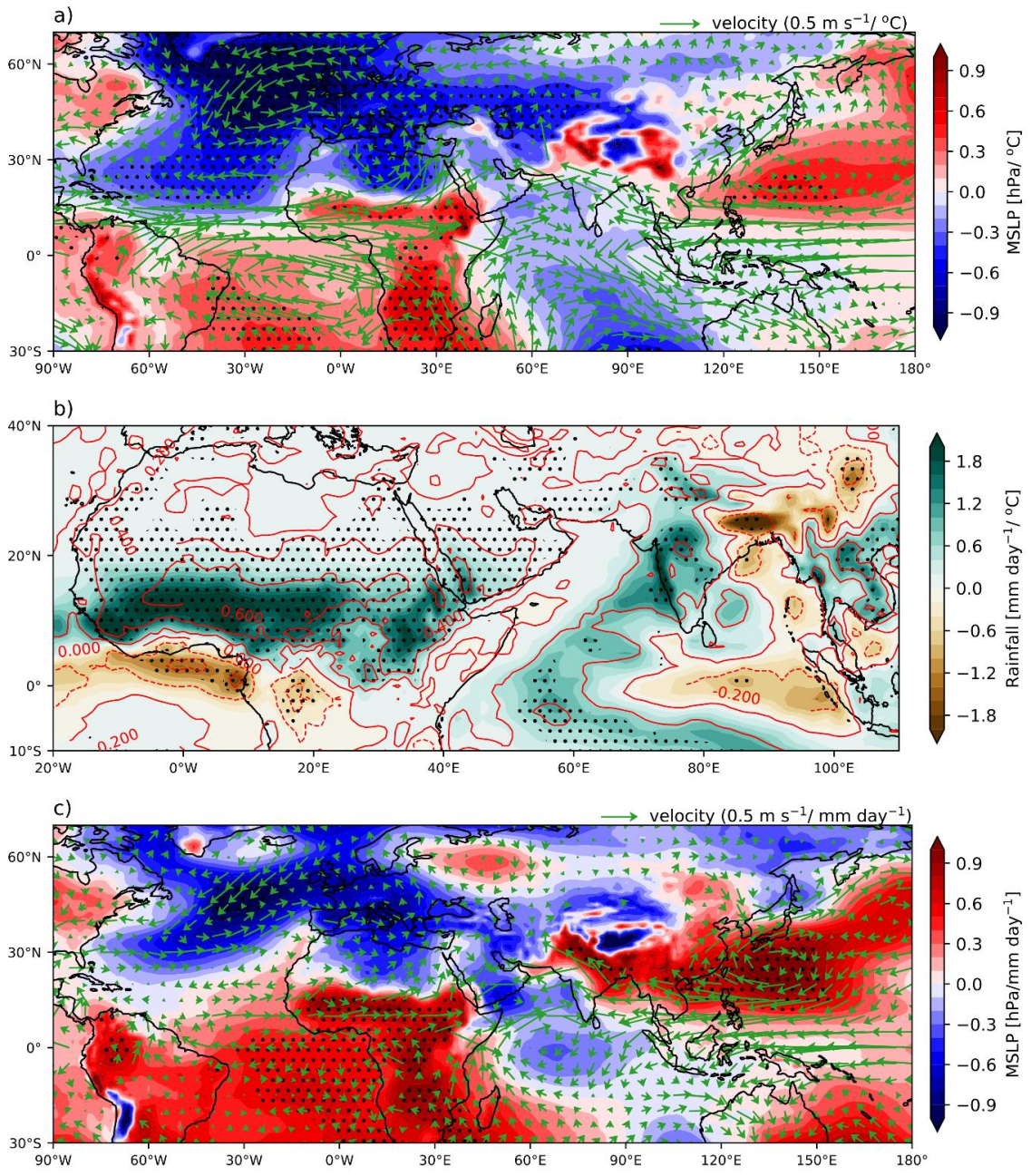


Figure 9: In (a), inter-model regression between future change in AMTG and future changes in MSLP (hPa/Deg C) and 850hPa wind (m/s/Deg C) at every grid point. In (b), inter-model regression between future change in AMTG and future change in rainfall at every grid point. In (c), inter-model regression between future change in ISM rainfall index (i.e., over 70°E-85°E, 8°N-22°N, mm/day/Deg C) and future changes in MSLP (hPa/ mm/day) and 850hPa wind (m/s/mm/day). Note that all the variables in all the panels are scaled by GMT of each model before doing the regression analysis. Also dotted regions in all the panels indicate regressions (for MSLP and rainfall) which are statistically significant at 90% level.

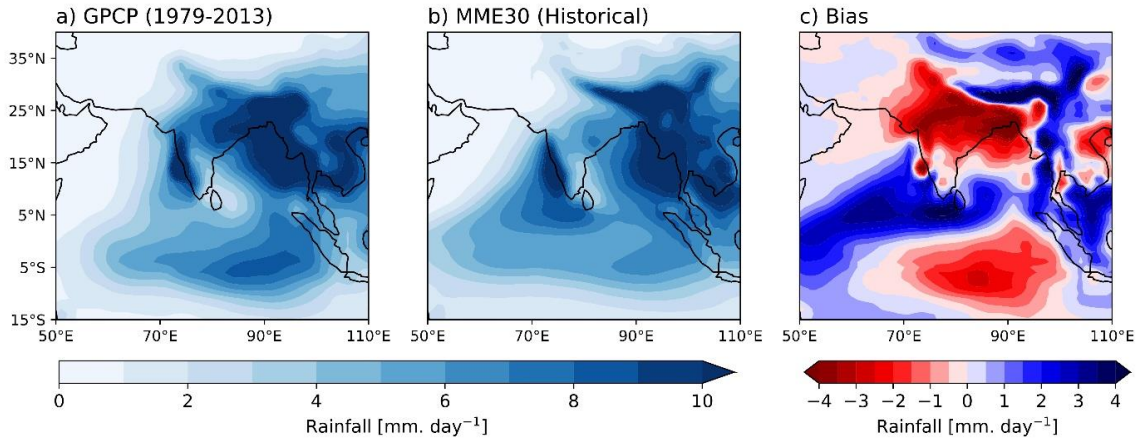


Fig 10: (a) JJAS climatological map of rainfall using GPCP dataset for the JJAS period (i.e., for the period of 1979-2013). In (b), same as (a), but using JJAS Climatology of rainfall using MME of 30 CMIP6 models (for the same period of 1979-2013). In (c), bias (relative to GPCP) in rainfall climatology for CMIP6 MME.

Tables:

Table 1. A list of the CMIP6 models utilized in the study.

Sr. No.	Model Name	Institute	Country	Resolution
1.	ACCESS-CM2	Commonwealth Scientific and Industrial Research Organization	Australia	250 km
2.	ACCESS-ESM1-5	Commonwealth Scientific and Industrial Research Organization	Australia	250 km
3.	BCC-CSM2-MR	Beijing Climate Center	China	100 km
4.	CAMS-CSM1-0	Chinese Academy of Meteorological Sciences	China	100 km
5.	CanESM5	Canadian Centre for Climate Modelling and Analysis	Canada	100 km
6.	CMCC-CM2-SR5	Fondazione Centro Euro-Mediterraneo sui Cambiamenti Climatici	Italy	100 km
7.	CMCC-ESM2	Fondazione Centro Euro-Mediterraneo sui Cambiamenti Climatici	Italy	100 km
8.	CNRM-CM6-1	National Center for Meteorological Research, Météo-France and CNRS laboratory	France	100 km
9.	CNRM-CM6-1-HR	National Center for Meteorological Research, Météo-France and CNRS laboratory	France	25 km
10.	EC-Earth3	Swedish Meteorological and Hydrological Institute/SMHI	Sweden	100 km
11.	EC-Earth3-CC	Swedish Meteorological and Hydrological Institute/SMHI	Sweden	100 km
12.	EC-Earth3-Veg-LR	Swedish Meteorological and Hydrological Institute/SMHI	Sweden	100 km
13.	FGOALS-f3-L	Chinese Academy of Sciences	China	100 km
14.	FGOALS-g3	Chinese Academy of Sciences	China	100 km
15.	FIO-ESM-2-0	First Institute of Oceanography, State Oceanic Administration	China	100 km

16.	GFDL-ESM4	National Oceanic and Atmospheric Administration, Geophysical Fluid Dynamics Laboratory	United States	50 km
17.	GISS-E2-1-G	Goddard Institute for Space Studies	United States	250 km
18.	GISS-E2-1-H	Goddard Institute for Space Studies	United States	250 km
19.	IITM-ESM	Centre for Climate Change Research, Indian Institute of Tropical Meteorology	India	250 km
20.	INM-CM5-0	Institute for Numerical Mathematics, Russian Academy of Science	Russia	100 km
21.	IPSL-CM6A-LR	Institute Pierre Simon Laplace	France	100 km
22.	KACE-1-0-G	National Institute of Meteorological Sciences/Korea Meteorological Administration	Korea	250 km
23.	MCM-UA-1-0	Department of Geosciences, University of Arizona	United States	250 km
24.	MIROC6	Japan Agency for Marine-Earth Science and Technology	Japan	100 km
25.	MPI-ESM1-2-LR	Max Planck Institute for Meteorology	Germany	250 km
26.	MRI-ESM2-0	Meteorological Research Institute	Japan	100 km
27.	NESM3	Nanjing University of Information Science and Technology	China	100 km
28.	NorESM2-LM	Norwegian Meteorological Institute	Norway	100 km
29.	NorESM2-MM	Norwegian Meteorological Institute	Norway	100 km
30.	TaiESM1	Research Center for Environmental Changes, Academia Sinica	Taiwan	100 km

Table 2: Definition of the indices used in the present study. The angle brackets are for spatial averaging of the corresponding variables over the relevant domains

Sr. No.	Indices used	Variables and Domains used for averaging
1.	Interhemispheric TS gradient (IHTG)	TS [25°N-90°N, 0° to 360°E] minus TS [60°S-90°N, 0° to 360°E]
2.	Atlantic Meridional TS Gradient (AMTG)	TS [40°W-10°W, 25°N-65°N] minus TS [40°W-10°W, 25°S-5°N]
3.	Low-Level Jet (NLLJ)	Zonal wind at 850 hPa [10°N–20°N, 55°E–65°E]
4.	South of the LLJ core position (SLLJ)	Zonal wind at 850 hPa [0°–10°N, 55°E–65°E]
5.	Tropical Easterly Jet (TEJ)	Zonal wind at 200hPa [40°E-100°E, 10°S-20°N]

Table 3: Intermodel standard deviation (SD, in mm/day) and Signal-to-Noise ratio (SNR) for the future change in moisture budget components averaged over ISM region (70°E-85°E, 8°N-22°N).

Moisture Budget terms	P'	E'	DY'	TH'	RES'
SD	0.820	0.153	0.539	0.517	0.411
SNR	1.878	1.295	0.706	1.862	-0.006

Funding

The authors have no funding reference to declare. This research did not receive any specific grant from funding agencies in the public, commercial, or not-for-profit sectors.

Data Availability

All the datasets used in this study are publicly available. The;] CMIP6 model datasets used for this study are available through the ESGF repository https://esgf-node.llnl.gov/search/cmip6/. The analysis was carried out utilizing open-source software tools such as the Climate Data Operators and Python (https://www.python.org/) for the computations and visualizations.

Conflict of interest

The authors have not disclosed any competing interests.

Author Contributions

Ajinkya M Aswale (AMA) conducted the analysis, handled software and visualization tools. SKP (Sooraj K P) and TP (Terray Pascal) formulated methodology, wrote the original draft, reviewed and edited the manuscript.

Supplementary Material

Click here to access/download
Supplementary Material
Supplementary-Figures.docx